HHS Public Access

Author manuscript

Sci Transl Med. Author manuscript; available in PMC 2020 May 13.

Published in final edited form as:

Sci Transl Med. 2020 April 15; 12(539): . doi:10.1126/scitranslmed.aax3799.

Interleukin 17 and senescent cells regulate the foreign body response to synthetic material implants in mice and humans

Liam Chung[1,2], **David R. Maestas Jr.**[2], **Andriana Lebid**[1], **Ashlie Mageau**[2], **Gedge D. Rosson**[3], **Xinqun Wu**[1], **Matthew T. Wolf**[1,2], **Ada J. Tam**[1], **Isabel Vanderzee**[2], **Xiaokun Wang**[2], **James I. Andorko**[1,2], **Hong Zhang**[2], **Radhika Narain**[2], **Kaitlyn Sadtler**[4], **Hongni Fan**[1], **Daniela Čiháková**[5], **Claude Jourdan Le Saux**[6], **Franck Housseau**[1], **Drew M. Pardoll**[1], **Jennifer H. Elisseeff**[1,2,*]

[1]Bloomberg~Kimmel Institute for Cancer Immunotherapy and Sidney Kimmel Comprehensive Cancer Center, Johns Hopkins University School of Medicine, Baltimore, MD 21231, USA.

[2]Translational Tissue Engineering Center, Wilmer Eye Institute and Department of Biomedical Engineering, Johns Hopkins University, Baltimore, MD 21287, USA.

[3]Division of Plastic Surgery, Department of Surgery, Johns Hopkins University, Baltimore, MD, USA.

[4]Section on Immuno-Engineering, National Institute for Biomed5ical Imaging and Bioengineering, National Institutes of Health, Bethesda, M6 D, USA.

[5]Department of Pathology, Johns Hopkins University, Baltimore, MD, USA.

[6]Department of Medicine, University of California, San Francisco, CA, USA.

Abstract

Medical devices and implants made of synthetic materials can induce an immune-mediated process when implanted in the body called the foreign body response, which results in formation of a fibrous capsule around the implant. To explore the immune and stromal connections underpinning the foreign body response, we analyzed fibrotic capsules surrounding surgically excised h+uman breast implants from 12 individuals. We found increased numbers of interleukin

*Corresponding author. jhe@jhu.edu.

Author contributions: L.C., J.H.E., D.M.P., and F.H. conceptualized the study. L.C. and J.H.E. discussed and formulated experimental design for the study. L.C., D.R.M., and A.L. contributed to analysis and interpretation of results. L.C., D.R.M., A.M., I.V., H.Z., R.N., M.T.W., X. Wang, A.L., and J.I.A. contributed to conducting experimental procedures. D.R.M., A.M., I.V., X. Wang, A.L., and J.I.A. assisted L.C. with the harvest and preparation of tissue for flow cytometry. M.T.W. assisted with histology staining and imaging. H.Z. assisted with bone marrow chimera experiments. G.D.R. provided human surgical discard samples. L.C., X. Wu, and H.F. assisted with animal breeding and genotyping. C.J.L.S., D.Č., and K.S. discussed and assisted in interpreting the results and commented on the manuscript. L.C., J.H.E., D.M.P., and F.H. wrote the manuscript with input from all co-authors.

Competing interests: L.C., J.H.E., and D.M.P. are coinventors on Provisional Patent Application no. 62/792,887, filed by Johns Hopkins University that is related to this work. J.H.E. holds equity in Unity Biotechnology and Aegeria Soft Tissue. J.H.E. is a member of the scientific advisory boards of ACell Inc., Camden Nexus Fund, and Histogenics. J.H.E. is a consultant for Vericel. D.M.P. is a consultant for Aduro Biotech, Amgen, Astra Zeneca, Bayer, Compugen, DNAtrix, Dynavax Technologies Corporation, Ervaxx, FLX Bio, Immunomic, Janssen, Merck, and Rock Springs Capital. D.M.P. holds equity in Aduro Biotech, DNAtrix, Ervaxx, Five Prime Therapeutics, Immunomic, Potenza, and Trieza Therapeutics. D.M.P. is a member of the scientific advisory boards for Bristol Myers Squibb, Camden Nexus II, Five Prime Therapeutics, and WindMil. D.M.P. is a member of the board of directors of Dracen Pharmaceuticals. All other authors declare that they have no competing interests.

Data and materials availability: All data associated with this study are in the paper or the Supplementary Materials. The IL17A and IL17F neutralizing antibodies were obtained from Amgen under a materials transfer agreement.

17 (IL17)–producing $\gamma\delta^+$ T cells and $CD4^+$ T helper 17 (T_H17) cells as well as senescent stromal cells in the fibrotic capsules. Further analysis in a murine model demonstrated an early innate IL17 respon+se to implanted synthetic material (polycaprolactone+) particles that was mediated by innate lymphoid cells and $\gamma\delta^+$ T cells. This was followed by a chronic adaptive $CD4^+$ T_H17 cell response that was antigen dependent. Synthetic materials with varying chemical and physical properties implanted either in injured muscle or sub-cutaneously induced similar IL17 responses in mice. Mice deficient in IL17 signaling established that IL17 was required for the fibrotic response to implanted synthetic materials and the development of $p16^{INK4a}$ senescent cells. IL6 produced by senescent cells was sufficient for the induction of IL17 expression in T cells. Treatment with a senolytic agent (navitoclax) that killed senescent cells reduced IL17 expression and fibrosis in the mouse implant model. Discovery of a feed-forward loop between the T_H17 immune response and the senescence response to implanted synthetic materials introduces new targets for therapeutic intervention in the foreign body response.

Abstract

One-sentence summary: Interleukin 17 and senescent cells regulate fibrosis in the foreign body response to synthetic material implants.

Editor's Summary:

Elucidating the foreign body response: Synthetic materials are the building blocks for medical devices and implants but can induce a foreign body response after implantation, resulting in fibrous scar tissue encompassing the implant. Here, Chung *et al.* define the role of interleukin 17 (IL17) and cellular senescence in driving the foreign body response. The fibrous capsule from excised breast implants contained IL17-producing T cells and senescent stromal cells. These findings were further validated in a murine model, and the authors found that blocking the IL17 path-way or eliminating senescent cells mitigated local fibrosis around the implant. This study presents new potential therapeutic targets to reduce fibrosis associated with the foreign body response.

INTRODUCTION

Synthetic materials serve as the building blocks of medical devices and implants. Synthetic materials were historically selected based on their physical properties such as mechanical strength and durability while at the same time inciting a minimal host immune response after implantation. Despite the many advances that medical implants bring to medicine, synthetic materials induce to varying extents an immune-mediated foreign body response (FBR), which leads to formation of a capsule of dense fibrous tissue surrounding the implant (1). Manipulating chemistry and surface properties can mitigate the FBR to a degree, but even a minor response can lead to device failure over time, which necessitates surgical removal. Whereas fibrosis may be leveraged to mechanically stabilize some devices such as orthopedic implants or stents, it can also lead to implant contraction in the case of hernia meshes and breast implants. Silicone breast implants are widely used in medical practice but develop fibrotic capsules that can necessitate replacement (2). Further, some recipients experience breast implant syndrome that includes increased risk of rheumatologic disorders (3). Recent reports on lymphomas arising around synthetic breast implants designed with a

surface to enhance fibrotic immobilization further validate the relevance of murine studies demonstrating the pro-carcinogenic potential of the FBR (4–6).

The classic FBR to synthetic materials was first defined in the 1970s (7–9). It is characterized by protein adsorption and complement activation followed by migration of pro-inflammatory innate immune cells, in particular, neutrophils and macrophages. Macrophages fuse to form foreign body giant cells, and fibroblasts are activated to secrete extracellular matrix, leading to formation of a fibrous capsule. Macrophages and the innate immune response are considered central to the FBR and fibrosis around implants; however, given that the innate and adaptive immune systems are intimately connected, it is possible that the adaptive immune system is also contributing to the FBR (10). Implantation of a synthetic material or clinical device may therefore affect immune memory and systemic immune responses with as yet unexplored clinical consequences.

T cells are a key component of the adaptive immune system and are increasingly recognized for their role in wound healing and tissue repair. $CD4^+$ helper T cells regulate bone, liver, and muscle repair processes (11–13). The T helper type 2 (T_H2) effector cells responding to pro-regenerative biological scaffolds secrete interleukin 4 (IL4) and direct the function of macrophages to promote muscle repair (13). The presence of T cells has been recognized in the FBR in animal models and surrounding clinical implants, but their nature, activation status, and role in the response is still largely unknown (10, 14). Adaptive responses that depend on T cells, which conventionally recognize major histocompatibility complex (MHC)–presented peptide antigens, have not been seriously considered in the response to synthetic materials despite their increasing association with fibrotic disease (15–17). Beyond T cells, the influence of other immune cell types such as γδ T cells and innate lymphoid cells (ILCs) in the regulation of the response to implanted synthetic materials, tissue damage, and fibrosis remains unexplored.

The connection between the immune response to synthetic materials, fibrosis, and senescent cells is also unexplored. Senescent cells are characterized by growth arrest but are far from quiescent. Accumulation of senescent cells is associated with age-related chronic diseases, but they also regulate development and wound healing (18, 19). Senescent cells exert their effects through the secretion of a senescence-associated secretory phenotype (SASP). The SASP includes many immunological cytokines that are associated with specific immune phenotypes (20). Clearance of senescent cells in transgenic mouse models or using senolytic drugs that kill senescent cells reduces fibrosis in idiopathic pulmonary fibrosis and reduces inflammation and disease symptoms in arthritis, diabetes, and cardio- vascular disease (21–24). Stromal cells such as fibroblasts, endothelial cells, and immune cells have all been found to undergo senescence in various tissues and disease states (25, 26).

Here, we identified adaptive immune regulators of the FBR to implanted synthetic materials. ILCs, $\gamma\delta^+$ T cells, and $CD4^+$ T cells were the primary sources of IL17 that promoted a fibrotic response to human breast implants and to a variety of implanted synthetic materials in murine models. We established the interplay between IL17 and senescent cells as a mechanism linking the chronic immune response to synthetic material implants and

excessive fibrosis. Therapeutic intervention targeting IL17 and senescence reduced fibrosis and inflammation in a mouse implant model.

RESULTS

Il17 secreted by T cells is associated with fibrosis in tissue surrounding human breast implants

Breast implants induce fibrosis that can cause capsular contraction that occasionally necessitates implant removal and replacement. We performed detailed analyses of the immune cells in multiple tissue samples surrounding implants removed from patients undergoing breast implant exchange surgery. All implants (total of 12 specimens) had an exterior silicone shell and were either temporary tissue expanders (8 specimens) filled with saline (or air) or permanent implants filled with silicone (2 specimens) or saline (2 specimens). Implant samples included those with both normal and textured surface properties. Most tissue expanders had a textured surface, whereas silicone- or saline-filled implants had a smooth surface. Peri-implant samples included tissues surrounding implants with both smooth and textured surface properties. Implants were originally placed adjacent to either adipose or muscle tissue depending on whether a pre-pectoral or sub-pectoral implantation technique was used. Average patient age was 56 (range of 41 to 70 years), and average implant residence time was 41 months (range of 1 to 360 months). For each implant capsule, we profiled up to four tissue sections including left anterior, left posterior, right anterior, and right posterior with respect to the anatomical position of the implant (fig. S1A).

Multiparametric flow cytometry of infiltrating $CD45^+$ leukocytes revealed the presence of large numbers of $CD3^+$ T cells in addition to myeloid populations of mononuclear phagocytes, dendritic cells, eosinophils, and granulocytes (fig. S1, B and C). Intracellular cytokine staining of $CD4^+$ T cells revealed significantly higher numbers of IL17-producing T cells (T_H17) compared to interferon γ (IFN γ) (T_H1)–producing T cells and IL4 (T_H2)–producing T cells in the tissue surrounding the implants ($P < 0.001$) (Fig. 1A). $\gamma\delta^+$ T cells ($CD45^+CD3^+\gamma\delta^+$) represented a high proportion of the total $CD3^+$ cells (mean ± SD, 16.97 ± 8.98%; fig. S1D) around the implants and expressed IL17 similar to the $CD4^+$ T cells. Immunofluorescence confirmed the presence of IL17 with concomitant nuclear staining of phosphorylated signal transducer and activator of transcription 3 (pSTAT3) that is essential for IL17 expression (Fig. 1B and fig. S1E) (27). Overall, these results support a consistent type 17 immune response (also termed type 3 immunity) (28) to human breast im- plants independent of the surface properties and implantation site, with both $\gamma\delta^+$ T cells and $CD4^+$ T cells serving as the primary contributors to IL17 production.

To investigate whether the T_H17/IL17 immune signature con- tributed to the fibrosis observed in human tissue surrounding the breast implants (Fig. 1B), we evaluated mRNA expression of *Col1a1* and *Col3a1* encoding collagen, transforming growth factor–β(*Tgf*β), and the fibroblast-specific protein *S100a4* (Fig. 1C and fig. S1F) (29–31). Expression of *Il17* mRNA positively correlated with expression of *Col1a1* ($R^2 = 0.5941$, $P = 0.0252$) and *Col3a1* ($R^2 = 0.5776$, $P = 0.0286$) mRNAs. The expression of *Il17* mRNA also correlated with mRNA expression of the fibrosis-related growth factor *Tgf*β ($R^2 = 0.7409$, $P = 0.0061$) (Fig. 1C). There was also a significant correlation between *Il17* mRNA expression and

STAT3 mRNA expression (R^2 = 0.7094, P = 0.0087), indicating a STAT3-dependent mechanism, further supporting the relevance of T_H17 T cells in the FBR. Together, these results suggest that the IL17 produced by $\gamma\delta^+$ and $CD4^+$ T cells may contribute to the regulation of fibrogenesis in response to breast implants.

Innate and adaptive immune responses sequentially contribute to chronic IL17 production in response to synthetic materials

To further investigate the role of IL17 in implant-associated fibrosis suggested by our findings from excised breast implants and to understand the mechanism linking the type 17 immune response to the FBR, we implanted synthetic materials into C57BL/6 mice. Materials were placed both subcutaneously and in a muscle wound to mimic surgical implantation and tissue trauma (fig. S2A). Poly (caprolactone) (PCL) was used as the primary model synthetic material because it induces a robust inflammatory response and is also a component of clinical implants (32). Results were validated with additional clinically relevant synthetic materials including poly- ethylene (PE), polyethylene glycol (PEG), and silicone.

Implantation of particulate PCL in surgical dermal and muscle wounds in mice increased IL17 expression in the tissue compared to wounds with no implant (saline controls) (Fig. 2A). We identified three primary cell sources of IL17 that evolved over time (Fig. 2, A to C). These were IL17-producing group 3 ILCs (ILC3s; $CD45^+CD3^-Thy1.2^+$) that respond quickly to danger-associated molecular patterns (DAMPs) and produce cytokines independently of T cell receptor (TCR) signaling; IL17-producing $\gamma\delta^+$ T cells ($\gamma\delta$T17) that recognize non-peptide antigens such as lipids, phosphoantigens, and carbohydrates; and adaptive $CD4^+$ T cells (T_H17) that are activated specifically through the $\alpha\beta$ TCR receptor (33).

At 1 week after implantation in the murine model, ILC3s and $\gamma\delta^+$ T17 cells were the primary source of IL17 (Fig. 2B). CD4+ T cells exhibited no differences between IFNγ, IL4, and IL17 expression 1 week after implantation as shown by intracellular staining (Fig. 2, A to C, and fig. S2, B and C). After 3 and 6 weeks after implantation, IL17 expression shifted from ILC3s and $\gamma\delta$T17 cells to T_H17 cells. Analysis of the immune response to PCL in IL17A–green fluorescent protein (GFP) reporter mice confirmed that $CD4^+$ T cells were the primary source of IL17A, and there was minimal IL17A expression in myeloid cells at 3 weeks after surgery (fig. S2D). At 3 weeks after surgery, $CD8^+$ T cell responses resolved, whereas $CD4^+$ T cells remained increased and continued to produce IL17 (fig. S2E). Both IL17A and IL17F expression significantly increased in T cells ($CD3^+CD11b^-$) sorted from PCL-associated tissue compared to saline-treated tissue at 1 week after surgery ($P < 0.0001$) (fig. S3A). Expression of *Rorc* (encoding the T_H17 transcription factor RORγt), *Il23r*, and *Dusp4* also increased in synthetic material–associated T cells, further supporting a T_H17 immune response. Last, gene expression analysis of the homogenized muscle tissue confirmed up-regulation of *Il17a* expression in response to PCL implants compared to no implants (saline controls) over time (fig. S3B). Expression of additional pro-inflammatory cytokines *Il1*β, tumor necrosis factor–α(*Tnf*α), and *Il23p19* also increased in implanted

muscle tissue (fig. S3B). These pro-inflammatory cytokines could drive immune activation and chronic inflammation through the dif- ferentiation and activation of T_H17 cells (34).

Although the degree and nature of the T_H17 and type 17 immune response varied depending on synthetic material composition and physical properties, a range of synthetic materials with diverse chemistry and physical properties activated this pathway in different tissue environments (Fig. 2, D and E). Flow cytometry and gene expression analysis confirmed the T_H17 response to multiple synthetic material types over 6 weeks of implantation in mice. At 3 weeks after implantation, flow cytometry showed expression of both IL17A and IL17F in $CD4^+$ T cells and ILC3s in response to PCL and PE, with most cells expressing both forms of the protein (Fig. 2D). At 6 weeks after implantation, gene expression of type 17 immunity–associated genes *Il1*β, *Tnf*α, *Il23*, and *Il17a* increased in response to PCL, silicone, and PEG (Fig. 2E). PCL particles implanted into the sub- cutaneous space with less tissue disruption or injected directly into muscle without a large wound also activated a type 17 response (fig. S3C). These results, combined with the data from human breast implants, suggested that the T_H17 response was activated in response to implants of various sizes, shapes, and textures in different tissue environments.

To determine whether the T_H17 response was mediated by TCRs, we generated bone marrow chimera mice by infusing wild-type CD45.1 and OTII-$Rag^{-/-}$ CD45.2 bone marrow into wild-type C57BL/6 CD45.2 mice after lethal irradiation (Fig. 2F). The OTII TCR transgenic $Rag^{-/-}$ $CD4^+$ T cells are specific for ovalbumin (OVA), so we tested whether there was nonspecific activation of OVA-specific T cells in the context of a highly diverse TCR repertoire of the CD45.1 cells in the muscle wound environment with or without PCL implantation. We found that both $CD45.1^+$ and $CD45.2^+$ donor immune cells responded to PCL implantation after 1 week. In the tissue and draining lymph nodes, $CD4^+$ T cells were primarily from the wild-type CD45.1 donor mice (figs. S3D and S4A). IL17 was expressed in wild-type CD45.1 $CD4^+$ T cells in response to PCL implantation, but was absent in the CD45.2 OTII-$Rag^{-/-}$ T cells. The capacity of OTII-$Rag^{-/-}$ T cells to undergo T_H17 differentiation was confirmed in vitro, so the failure to produce IL17 in response to synthetic material implants did not represent an intrinsic defect in their ability to undergo differentiation to T_H17 cells (fig. S4B). This suggests that the IL17 production by $CD4^+$ T cells in response to PCL implantation was antigen specific. As previously described, synthetic materials can modulate the T cell response to antigen, thereby acting as an adjuvant. Splenocytes from OTII mice cultured in vitro with OVA in combination with PCL or PE for 48 hours showed increased T cell proliferation and cytokine production compared to splenocytes from OTII mice cultured without synthetic materials (Fig. 2G and fig. S4C). At 6 weeks after surgery, we detected elevated immunoglobulin G1 (IgG1) in the serum of mice implanted with PCL compared to saline controls, highlighting a B cell response and antibody class switching with implantation of synthetic materials (fig. S5A).

Given that our data supported engagement of the adaptive immune system in the FBR, we evaluated whether there was an immune memory response to implantation of synthetic materials. Mice were implanted with PCL in the muscle and after 1 week were rechallenged with a second PCL implant in the subcutaneous space on the flank of the mouse. One week after the subcutaneous implant, expression of *Il17a* was evaluated in animals receiving a first

implant in the muscle or no previous implant. Previous exposure to a PCL implant (PCL primed) enhanced *Il17a* expression in the tissue around the subcutaneous implant when compared to subcutaneous implants in mice that did not receive a previous PCL implant (that is, animals with saline-treated muscle wounds) (fig. S5B). Treatment with IL6 neutralizing antibodies completely mitigated the increase in IL17A in the subcutaneous implants regardless of PCL priming status (fig. S5B). We further assessed whether there was a PCL antigen-specific response capable of inducing immunological memory using a combination of in vivo and in vitro experiments. Splenocytes were harvested from mice treated with PCL or saline-treated controls after 3 weeks. After labeling with a dye to detect cell proliferation, we challenged the splenocytes with PCL in culture. Splenocytes from mice previously implanted with PCL (primed) showed higher proliferation at 96 hours in culture compared to cells from mice that did not receive a PCL implant (not primed) (fig. S5C).

Chronic IL17 production in response to synthetic material implants promotes fibrosis

T_H17 immune responses are implicated in fibrotic diseases in multiple tissue types including skin, heart, lung, and liver, although they have not been studied in the context of FBR (35–38). In wild-type mice that demonstrated a type 17 immune response, the expression of fibrosis-related genes after surgery changed over time (fig. S5D). Without an implanted synthetic material, expression of the extra- cellular matrix genes *Col1a1* and *Col3a1* initially increased after surgery and then decreased after 6 weeks as normal healing progressed, and tissue was repaired (fig. S5D). The presence of the PCL implant increased expression of *Col3a1* and the fibrosis-associated gene *S100a4* after 6 and 12 weeks, respectively (fig. S5D). Masson's trichrome stain and immunohistochemistry confirmed increased collagenous extracellular matrix and α smooth muscle actin protein (αSMA) surrounding the implanted PCL particles (Fig. 3A), features typical of the FBR and fibrotic capsule formation.

To evaluate whether fibrosis associated with the FBR to synthetic materials was IL17 dependent, we compared the implant response in $IL17A^{-/-}$ and $IL17RA^{-/-}$ mice with that in wild-type mice. We found that expression of fibrosis-related genes *S100a4*, *Tgf*β, *Col1a1*, and *Col3a1* decreased in both $IL17A^{-/-}$ and $IL17RA^{-/-}$ knockout mice implanted with PCL particles compared to wild-type mice (Fig. 3B and fig. S6A). The quantity, composition, and organization of extracellular matrix visible around the PCL particles decreased in the knockout animals (Fig. 3A). In addition, αSMA immuno-fluorescence was absent in knockout mice that lacked IL17 signaling (Fig. 3A). Picrosirius red staining visualized with a polarized lens produces birefringence that is proportional to collagen fiber diameter; larger collagen fibers are green to yellow (39). Picrosirius red staining showed reduced collagen matrix, capsule formation, and thinner fiber diameter in knockout mice that lacked IL17 signaling compared to wild-type mice at 12 weeks after surgery (Fig. 3C). Tissue repair and recovery was not impaired in the IL17A−/− and IL17RA−/− mice as assessed by treadmill testing (fig. S6B). In addition, expression of the inflammasome-associated genes *Nlrp3* and *Il1*β was reduced in PCL-implanted $IL17RA^{-/-}$ mice but not in implanted $IL17A^{-/-}$ mice or wild-type mice (fig. S6C). We also found decreased *Smad2*, *Smad3*, and *Smad4* gene expression in $IL17RA^{-/-}$ mice with implanted PCL particles compared to implanted wild-

type mice; this was not observed in implanted IL17A$^{-/-}$ mice (fig. S6D). These findings further support the IL17-dependent nature of the FBR to synthetic materials.

We next assessed the myeloid response associated with PCL implantation in the IL17A$^{-/-}$ and IL17RA$^{-/-}$ knockout mice. The number of neutrophils and macrophages increased in muscle tissue implanted with synthetic materials (fig. S7C). Macrophages sorted from tissue implanted with PCL particles expressed higher amounts of profibrotic stimulating factors that directly activate fibroblasts including *Tgf*β, platelet-derived growth factor α (*Pdgf*α), and vascular endothelial growth factor α (*Vegf*α) (fig. S7A). Whereas the number of monocytes in the IL17A$^{-/-}$ and IL17RA$^{-/-}$ implanted mice did not change, the proportion of MHC class II (MHCII)^{high}–expressing and MHCII^{low}-expressing macrophages was altered. MHCII^{high} macro- phage numbers in the implanted IL17RA$^{-/-}$ mice were similar to those in the wild-type control mice without implants. MHCII^{low} macrophage numbers significantly decreased in implanted IL17A$^{-/-}$ and IL17RA$^{-/-}$ mice compared to implanted wild-type control mice ($P < 0.005$) (fig. S7, B and C). Neutrophils (CD11b^{+}Ly6c^{+}Ly6g^{+}) and macrophages (CD11b^{+}F4/80^{+}) decreased in the IL17A$^{-/-}$ and IL17RA$^{-/-}$ implanted mice compared to implanted wild-type mice 12 weeks after surgery (fig. S7, B to D). Flow cytometry and immuno- fluorescence confirmed fewer neutrophils in the IL17A$^{-/-}$ and IL17RA$^{-/-}$ mice implanted with PCL particles compared to implanted wild-type mice (fig. S7C).

Results from the IL17A$^{-/-}$ and IL17RA−/− knockout mice suggested that blocking IL17 signaling may reduce FBR-associated fibrosis without negatively affecting healing. We therefore sought to determine the therapeutic potential of blocking IL17 on fibrosis. Given that IL17A and IL17F were both produced in response to the implanted synthetic material and the IL17RA$^{-/-}$ mice showed a greater reduction in fibrosis compared to IL17A$^{-/-}$ mice, we evaluated delivery of neutralizing antibodies against IL17A and IL17F to test the impact of functional neutralization of IL17 signaling on fibrosis. Mice were treated with neutralizing antibodies against IL17A and IL17F 4 weeks after synthetic material implantation, with dosing every other day for 1 week for a total of five injections. One week after neutralizing antibody treatment, *IL17* and *IL6* mRNA expression decreased; expression of fibrosis-associated genes *Tgf*β and *Col1a1* also decreased (Fig. 3D). Immunofluorescence staining of αSMA also decreased, further suggesting that there was a reduction in fibrosis (Fig. 3C). Histologically, collagen density and fiber organization decreased after treatment with neutralizing antibody compared to isotype control antibody (Fig. 3C). Picrosirius red staining and quantification demonstrated that neutralizing antibodies against IL17A and IL17F modulated extracellular matrix organization and reduced fibrosis in a manner similar to that seen in the IL17A$^{-/-}$ and IL17RA−/− knockout animals.

p16^{INK4a} senescent cells develop during FBR, and senolytic drugs reduce fibrosis

IL6 is a critical mediator contributing to the differentiation of T_H17 cells. Given that IL6 is associated with the SASP produced by senescent cells, we investigated whether senescent cells were a potential source of IL6 contributing to chronic IL17 production and fibrosis (18). Senescent cells are characterized by expression of *p16^{INK4a}*, *p21*, and SASP factors (40–42). Consistent with the kinetics of fibrosis devel- opment, *p16^{INK4a}* expression

significantly increased from 6 to 12 weeks after PCL implantation in mice compared to control animals receiving saline ($P < 0.0001$ at 6 weeks; $P < 0.01$ at 12 weeks) (Fig. 4A). *p16*^{INK4a}-positive cells were localized to the peri-implant region and exhibited a fibroblastic morphology with a single nucleus (Fig. 4B and figs. S7E and S8A). Fibroblasts sorted by flow cytometry from PCL-implanted tissue expressed significantly higher *p16*^{INK4a} compared with fibroblasts from control mice treated with saline, whereas sorted macrophages did not express *p16INK4a* ($P < 0.001$) (figs. S7A and S8B). Senescent cell development was abrogated in both the IL17A$^{-/-}$ and IL17RA$^{-/-}$ mice, where *p16*^{INK4a} expression in PCL-implanted tissue was similar to that of tissue from control mice without implants at 12 weeks, demonstrating that senescent cell development depended on IL17 (Fig. 4C). All synthetic materials tested induced *p16*^{INK4a} expression to varying degrees, suggesting that the response was materials independent (Fig. 4D). To further validate and define relevance for the association of senescent cells with fibrosis and the FBR, we evaluated patient tissue from breast implant exchange surgery. A large number of p16^{INK4a}-positive cells were present in the tissue surrounding the breast implants (Fig. 4E). Gene expression analysis of tissue surrounding the implants also showed a positive correlation between expression of *Il17* and *p16*^{INK4a} ($R^2 = 0.7636$, $P = 0.0046$) and *Il17* and *p21* ($R^2 = 0.8253$, $P = 0.0018$; Fig. 4E).

To further study the role of senescence in regulation of the FBR, we injected γ-irradiated senescent fibroblasts locally together with PCL particles into wounded muscle in a volumetric muscle loss mouse model. Addition of senescent fibroblasts to implanted PCL particles resulted in increased *Il17a* mRNA expression compared to mice that received normal (non-irradiated) fibroblasts with implanted PCL particles (fig. S8C). To determine the role of IL6 secreted by the transplanted senescent cells, we injected senescent fibroblasts into a local injury site in IL6$^{-/-}$ mice that had received PCL implants. In this model, the source of IL6 was limited to the injected senescent cells and was not produced by host senescent cells that were found around the implanted PCL particles. Mice that received senescent cells along with the implanted PCL particles showed up-regulated *Il17a* mRNA expression (fig. S8D). However, treatment with IL6 neutralizing antibody diminished *Il17a* mRNA expression to base- line levels (fig. S8D). This observation suggested that senescent cells may be key drivers of the IL17 response through their SASP and specifically IL6. To determine whether clearance of senescent cells associated with the FBR could reduce fibrosis, we administered the senolytic agent navitoclax (ABT-263) that selectively kills senescent cells (25, 43). The senolytic drug navitoclax was administered alone and in combination with neutralizing antibodies against IL17A and IL17F 4 weeks after synthetic material implantation. This time point for treatment was selected as it coincided with the peak in *p16*^{INK4a} expression in PCL-implanted mice compared to saline control mice (Fig. 4A). A reduction in αSMA immunofluorescence staining around implanted PCL particles suggested reduced fibrosis activity after senolytic drug treatment (Fig. 4F). One week after navitoclax treatment (6 weeks after PCL implantation), expression of *p16*^{INK4a} decreased, confirming senolysis and clearance of senescent cells ($P < 0.0001$) (Fig. 4G). Concomitant with p16^{INK4a} and αSMA reduction, *Il17a*, *Il6*, *Tgfβ*, *S100a4*, *Col1a*, and *Col3a* mRNA expression was decreased after navitoclax treatment. Expression of these genes decreased even further when the senolytic drug was co-administered with neutralizing antibodies

against IL17A and IL17F (Fig. 4G). Altogether, these findings suggest that cellular senescence sustains excess fibrosis and connects chronic IL17 production and fibrogenesis during the FBR.

DISCUSSION

Medical implants derived from synthetic materials can be associated with the FBR that not only impairs implant function and longevity but may also affect the host. There are anecdotal reports of systemic illnesses associated with orthopedic and soft tissue implants, most notably breast implant syndrome (44, 45). With only local inflammatory components considered relevant to the FBR, direct correlation of implant responses with systemic immune pathologies has been difficult to connect. Preclinical and clinical observations have noted the presence of T cells around implants, but their relevance to the fibrotic inflammatory response has been unclear (14, 46). Here, we present evidence of an IL17 inflammatory response and cellular senescence in the FBR to implanted synthetic materials and implicate them in the associated fibrotic response.

T cells are increasingly recognized for their role in determining repair pathways after tissue damage. We observed a T_H17 response to implanted synthetic materials with multiple chemistries in different anatomical locations in mice. B cells and their antibody production have already been associated with tissue damage and more recently with synthetic materials (47–49). For example, a B cell response to synthetic materials was discovered after implantation in the intraperitoneal cavity of mice. Moreover, the response was independent of the chemistry and physical properties of the implanted material (49). In our studies, we used particles of different synthetic materials that are used in devices and implants clinically. These particulates had different sizes, textures, and surface properties and could activate rapid, inflammasome-mediated innate immune responses (50). Mechanical forces created by implants and the related mechano- transduction of those signals can regulate cellular behavior, which may be particularly relevant for larger clinical implants (51). Synthetic material properties such as stiffness, size, and surface topography can influence cell behavior and cytokine production (52–54). Mechanical strain can also modulate fibroblast proliferation and gene expression and may therefore be an important factor in promoting IL17 production and senescence in the FBR. Further studies may elucidate unique aspects of the IL17 immune response with different synthetic materials and implant designs.

The induction of IL17-mediated inflammation has been implicated in tissue fibrosis. For example, IL17 is a central contributor to pathogenic lung and liver fibrosis (55, 56). Whereas T_H17 responses are a mechanism to combat extracellular pathogens, they are also associated with autoimmune diseases. For example, T_H17 cells are implicated in rheumatoid arthritis and Sjogren's syndrome, and therapies inhibiting IL17 ameliorate disease symptoms. Induction of a T_H17 immune response to synthetic materials is supported by the chronic neutrophil response to synthetic materials, as IL17 induces chronic neutrophilia. Multiple studies have now demonstrated a negligible impact of neutrophil depletion on fibrosis around implanted synthetic materials, suggesting that they are not inducing fibrosis (49, 57).

Our finding of senescent cells in the FBR presents a mechanism for the sustained type 17 inflammation and fibrosis around implants and suggests a new therapeutic target. Senolytic compounds are being developed to treat many age-related diseases including arthritis, cardio-vascular disease, and Alzheimer's disease (58, 59). Clinical studies testing senolytic drugs in idiopathic pulmonary fibrosis are already showing efficacy, and more clinical studies are ongoing (60, 61). The SASP secreted by senescent cells includes cytokines associated with a T_H17 immune response including IL6 and IL1β. The loss of senescent cells in the IL17A$^{-/-}$ and IL17RA$^{-/-}$ knockout mouse models further supports the connection between IL17 production and senescent cell formation. It is possible that the T_H17 response is being driven locally by synthetic material antigens, possibly facilitated by the senescent cells, as appears to be the case in post-traumatic osteoarthritis (62). The morphology of the p16^{INK4a}-positive cells found around the implants in mice and surgically removed breast implants from people appeared to be fibroblastic. Sorted fibroblasts from mice expressed higher p16^{INK4a}, suggesting that stromal fibroblasts are a mediator of senescence in the FBR. Other, as yet unidentified, cell types may become senescent during the FBR. Further studies using new genetic tools will help to elucidate the source and phenotype of senescent cells along with possible connections to myofibroblasts.

Canonical activation of T cells requires presentation of antigen and costimulatory factors. The lack of CD4$^+$ T cell responses to implanted PCL in the chimeric OTII-Rag$^{-/-}$ T cells confirms that the T_H17 implant response is antigen dependent. One explanation for an antigen-specific T cell response to implanted synthetic materials that do not contain protein is a low-level chemical derivatization of self-protein by components of the synthetic material such that they now appear as "non-self." The finding of IgG in response to implantation of a synthetic material in mice supports this hypothesis, as haptenization of proteins is necessary for the T cell help required for antibody switching in activated hapten-specific B cells (63, 64). Combinations of a synthetic material with host proteins can activate T cells as has been reported for titanium implant debris that creates a metal-protein complex that can elicit T cell responses (65). Addition of an implant in the context of tissue damage may modulate the natural adaptive immune response by modifying self-antigens or affecting antigen presentation. Last, there is evidence that T cells can specifically respond to non-peptidic repeating structures such as sugars and lipids and thus may recognize repeating polymer structures (66, 67). Regardless of the antigen or combination of antigens, the type 17 immune response is activated during the FBR and directs key aspects of the FBR, suggesting that targeting this pathway may have therapeutic benefits.

There are several limitations to our study. Although correlations were made between human breast implants and mouse models, the murine models used here cannot fully recapitulate the impact of device implantation in people. The mechanism of activation and specific antigens that led to the differentiation of CD4$^+$ T cells toward a type 17 adaptive immune response, as well as the details of the γδ$^+$ T cell response, remain to be elucidated. Synthetic materials can be manipulated in many ways to modulate their activity in vivo, including surface chemistry and topography, size, and mechanical properties. However, our study did not systematically evaluate the impact of these variables. For better clinical understanding, future studies will need to investigate how multiple immunomodulatory environmental factors can affect the T_H17 and senescence responses to synthetic material implants.

MATERIALS AND METHODS

Study design

We aimed to investigate senescence and IL17-driven FBR in response to synthetic material implants in people and to study in detail the mechanisms of the FBR in mice. We performed detailed analysis of the immune cells in multiple tissue samples surrounding breast implants removed from patients undergoing breast implant exchange surgery using flow cytometry and immunofluorescence staining. To further investigate the role of IL17 in implant-associated fibrosis, we implanted synthetic materials into C57BL/6 mice using a volumetric muscle loss model. Synthetic materials in particulate form were placed both subcutaneously and in a muscle wound to mimic surgical implantation and tissue trauma. PCL, PEG, and silicone were used as implant materials. To evaluate whether fibrosis associated with the FBR to the implanted materials was dependent on IL17 production, we compared the implant response in IL17A−/− and IL17RA−/− knockout mice with that in wild-type mice. Researchers were not blinded to delivery of synthetic material implants because of the obvious appearance of the materials before and after implantation. All experiments were performed using 6- to 8-week-old female mice (n = 3 to 9 as indicated in figure legends). We did not exclude any outliers from the analysis.

Clinical samples

Tissue was acquired from patients undergoing breast implant exchange or replacement surgeries (n = 12, Johns Hopkins University Institutional Review Board exemption IRB00088842); the breast implants were surgical discards that were deidentified. For each patient, up to four tissue sections were profiled, including the left anterior, left posterior, right anterior, and right posterior with respect to the anatomical position of the implant (fig. S1A). Each section was weighed, and 0.25 g of tissue was dissected for histology. Remaining tissue was analyzed depending on the available quantity; quantitative real-time polymerase chain reaction (qRT-PCR) assay (<1 g), flow cytometry (1 to 2 g), or both (>2 g). In this study, eight samples were used for qRT-PCR, and five samples were used for flow cytometry from different individuals (n = 12). Peri-implant samples included tissues surrounding implants with both smooth and textured surface properties. All implants had a silicone shell and were either temporary tissue expanders filled with saline or air or permanent implants filled with silicone or saline. Average patient age was 56 years old (range of 41 to 70 years old), and the average implant residence time was 41 months (range of 1 to 360 months).

Surgical procedures and implantation

All animal procedures were performed in accordance with an approved Johns Hopkins University Institutional Animal Care and Use Committee protocol. Female mice were aged 6 to 8 weeks old. Several strains were used, including wild-type C57BL/6j (The Jackson Laboratory, stock #00064), Rag2/OTII (Taconic, stock #11490), and IL17A$^{-/-}$ and IL17RA$^{-/-}$ knockout mice (courtesy of Y. Iwakura, University of Tokyo, Tokyo, Japan and T. Mustelin, Amgen, Seattle, respectively). Defects in muscle for material implantation were created as previously described (68). The resulting bilateral muscle defects were filled with 30 mg of a synthetic material.

Synthetic materials tested included PCL (particulate, M_n = 50,000 g/mol; mean particle size, <600 μm; Polysciences), ultrahigh molecular weight PE (particulate, M_n = 5,000,000 g/mol; mean particle size, 150 μm; Goodfellow), medical-grade silicone (sheet, Summit Medical), and PEG hydrogels. PEG hydrogels were made with PEG-diacrylate (PEG-DA; M_n = 3400). PEG-DA (Polysciences) in phosphate-buffered saline (PBS) at 10% (w/v) concentration was mixed with photoinitiator [Irgacure 2959 solubilized to 10% (w/v) in 70% ethanol] to a final concentration of 0.05%. A 50-μl volume solution was cast onto each well of a flat-bottom 96-well plate. The solution was photocrosslinked via ultraviolet (UV) light for 30 min to form a hydrogel sheet. Both silicone and PEG hydrogels were morselized into particles with a scalpel and placed into the defect. Control implants were injected with 50 μl of PBS (as a no-implant control). All materials were UV-sterilized before use. Directly after surgery, mice were given subcutaneous carprofen (Rimadyl, Zoetis) at 5 mg/kg for pain relief. Mice were euthanized, and their implants were extracted at different time points: 1, 3, 6, or 12 weeks after surgery. Additional modes of implantation were subcutaneous and intramuscular injection. Briefly, synthetic materials were implanted subcutaneously (30 mg) on both flanks of the mice or injected directly into the quadriceps muscles through a 16-gauge syringe (5 mg of materials).

qRT-PCR assay

Total RNA was isolated from whole tissue using TRIzol reagent and Qiagen's RNeasy kits. qRT-PCR was performed using Power SYBR Green Master Mix (Applied Biosystems) or TaqMan Gene Expression Master Mix (Applied Biosystems) according to the manufacturer's instructions. Briefly, 2 μg of total RNA was used to synthesize complementary DNA (cDNA) using SuperScript IV VILO Master Mix (Thermo Fisher Scientific). The cDNA concentration was set to 50 ng per well (in a total volume of 20-μl PCR). The qRT-PCRs were performed on the StepOne Plus Real-Time PCR System (Thermo Fisher Scientific) using the manufacturer's recommended settings for quantitative and relative expression. Primers used for qRT-PCR are listed in tables S1 to S3.

Flow cytometry

Tissue samples were obtained by cutting the quadriceps femoris muscle from the hip to the knee. Tissues were finely diced and digested for 45 min at 37°C with 1.67 Wünsch U/ml Liberase TL (Roche Diagnostics) and deoxyribonuclease I (0.2 mg/ml; Roche Diagnostics) in RPMI 1640 medium (Gibco). The digested tissues were ground through 100-μm cell strainers (Thermo Fisher Scientific) with excess RPMI and then washed twice with 1× DPBS (Dulbecco's phosphate-buffered saline). Percoll (GE Healthcare) density gradient centrifugation was used to enrich the leukocyte fraction and remove debris from the muscle samples. For intracellular staining, cells were stimulated for 4 hours with Cell Stimulation Cocktail (plus protein transport inhibitors) (eBioscience) diluted in complete culture media [IMDM (Iscove's modified Dulbecco's medium) supplemented with 5% fetal bovine serum]. Cells were washed and surface-stained, followed by fixation/permeabilization (Cytofix/ Cytoperm, BD), and then stained for intracellular markers. Flow cytometry was performed using Attune NxT Flow Cytometer (Thermo Fisher Scientific). The enriched cells were washed and stained with the antibody panels listed in tables S4 and S5.

Immunofluorescence

IL17 and p16 were stained using tyramide signal amplification method with Opal-570 (PerkinElmer, catalog no. FP1488001KT) and Opal-650 (PerkinElmer, catalog no. FP1496001KT), respectively. Briefly, after blocking with bovine serum albumin, the first primary antibody was incubated at room temperature for 30 min, followed by 10 min of incubation with horseradish peroxidase (HRP) polymer-conjugated secondary antibody, and 10 min of Opal-650. Unbound antibodies were stripped by microwaving in citrate buffer for 15 min to allow introduction of the next primary antibody (with different Opal dyes). Slides were then counterstained with 4′,6-diamidino-2-phenylindole (DAPI) for 5 min before being mounted using DAKO mounting medium (Agilent, catalog no. S302380–2). Imaging of the histological samples was performed on a Zeiss Axio Imager A2 and Zeiss AxioVision software version 4.2. Subsequent images were stitched together using ImageJ2 software.

IL17 neutralization, IL6 blocking antibody, and senolytic treatment

Mice received 100-μl intraperitoneal injections of anti-IL17A (100 μg/ml, catalog no. P13705.15) and anti-IL17F (100 μg/ml, catalog no. P56220.17) (provided by Amgen) or isotype control (rat IgG2a, Thermo Fisher Scientific, catalog no. 02–9688) every other day for a week. IL6 blocking antibody was administrated at 100 μg/ml (BioXCell, clone MP5–20F3) per mouse per day for five consecutive days. For senolytic treatment, mice received intra-peritoneal and intramuscular injections of navitoclax (100 mg/kg; Selleckchem, catalog no. HY-10087) for five consecutive days or vehicle control [5% dimethyl sulfoxide (DMSO) and 3% Tween 80 in PBS]. Co-administration of anti-IL17A/F and senolytic treatment was also evaluated. All mice received treatments at 4 weeks after surgery for a total of five injections (one injection per day per mouse) and were harvested in the following 2 weeks.

Bone marrow chimera mice

Three million bone marrow cells from each donor mouse [CD45.1 wild-type mice (The Jackson Laboratory, stock #002014) and CD45.2 OTII-RagKO mice (Taconic, stock #11490)] were injected intra-venously into lethally irradiated (1200 cGy: twice at 600 cGy at 4-hour intervals) 6-week-old recipients. Bone marrow reconstituted mice were rested for 3 months before the VML (volumetric muscle loss) procedure.

Histopathology

Tissues were harvested and fixed in 10% neutral buffered formalin for 24 hours before stepwise dehydration in EtOH, cleared with xylenes, and embedded in paraffin. Samples were sectioned as 7 μm slices using a Leica RM2255 microtome. Samples were stained for histopathological examination using Masson’s trichrome (Sigma-Aldrich), hematoxylin and eosin (Sigma-Aldrich), and pi-crosirius red (Abcam) stains according to standard manufacturer protocols.

Treadmill testing

Before testing, mice were trained on a treadmill apparatus at 5 m/min for 5 min. Mice were run to exhaustion starting at the speed of 5 m/min, with 1 m/min speed increase every minute. Exhaustion was determined when the mouse stopped running and stayed on the

pulsed shock grid for a continuous 30 s. All mice were evaluated at 3, 6, and 12 weeks after injury.

Antibody titer

PCL particles were dissolved in chloroform to coat the bottom of 96-well plates (20 mg/ml). Sera collected 3, 6, and 12 weeks after injury were serially diluted (in the range of 1:50 to 1:102,400) in ELISA Assay Diluent (BioLegend, catalog no. 421203). Before loading, the PCL-coated plate was blocked with the assay diluent for 1 hour.

After blocking, each dilution of the serum sample was loaded into the plate and incubated for 2 hours. After washing, biotin anti-mouse IgG1 or IgM or IgA was added to capture the bound antibody for 1 hour, followed by washing. Streptavidin solution was added to the wells and incubated for 30 min. Trimethylboron substrate was used for HRP detection and stopped with H_2SO_4. Absorbance was read at 450 and 570 nm (background control).

T_H17 in vitro skewing assay

Naïve CD4+ T cells were isolated from mouse spleens and lymph nodes using the Miltenyi Biotec Naïve $CD4^+$ Isolation Kit according to the manufacturer's protocol. Cells were differentiated using the CellXVivo Mouse T_H17 Cell Differentiation Kit (R&D Systems, catalog no. CDK017) according to the manufacturer's protocol. Cells were cultured for 5 days (refreshed the differentiation media at day 3). On day 5, cells were stimulated with Cell Stimulation Cocktail for 4 hours before cytokine staining and examined using flow cytometry.

Cell proliferation assays

Primary splenocytes were isolated from OTII transgenic mice. Cells were labeled with Cell Trace Violet Cell Proliferation Kit (Invitrogen) according to the manufacturer's protocol. Three million cells per well were seeded into six-well plates and grown in RPMI supplemented with 10% fetal calf serum (Gibco), nonessential amino acids, sodium pyruvate (Invitrogen), and penicillin-streptomycin (Invitrogen). At the same time, OVA and biomaterials (PCL or PE, 10 mg per well) were introduced into culture. After 48 hours, cells were harvested and analyzed using flow cytometry.

Rechallenge experiments

Mice were given an initial challenge of PCL or saline control treatment, locally delivered into the VML injury space (priming). The mice were then challenged/rechallenged with PCL by subcutaneous implant 1 week after the initial injury and treatment. In brief, following anesthesia, both flanks of mice were shaved and disinfected with 70% ethanol. A sterile blade was used to make a 5-mm incision through the skin only. Sterile forceps were used to separate the skin to create about 4 cm × 4 cm subcutaneous pocket. About 10 mg of PCL materials was placed inside the pocket on each side. The skin was then apposed and stapled. At 2 weeks after VML, we harvested the cells infiltrating the SubQ implants and assessed their gene expression by qRT-PCR.

Statistical analysis

The nCounter differential gene expression system was used to assess readable transcripts via the nanoStringPanCancerImmune Profiling Panel. We used thenSolver software (version 3.0, nanoString Technologies Inc.). All analyses of qRT-PCR data used the Livak method, wherein $\Delta\Delta C_t$ values are calculated, and then reported as relative quantification values calculated by $2^{-\Delta\Delta Ct}$ (69). Treatment data points are normalized to either healthy or saline-treated controls. $\beta 2M$ was used as the reference gene. In the flow cytometry analyses, the total number of cytokine-secreting cells was computed using FlowJo software and displayed as the mean ± SD. Two-way analyses of variance (ANOVAs) were performed using GraphPad Prism v6, with statistical significance designated at $P \leq 0.05$. Linear regression was used for the analysis of association between gene expression in human tissue samples.

Supplementary Material

Refer to Web version on PubMed Central for supplementary material.

Acknowledgments:

We thank Amgen for the IL17A and IL17F neutralizing antibodies. We also acknowledge S. Ganguli for assistance with NanoString multiplex gene expression platform, Y. R. Gonzalez and K. R. Wagner for help with the treadmill testing, and C. Sears for providing the IL17 knockout mice and helping with the experiments.

Funding:

This work was funded, in part, by the Bloomberg~Kimmel Institute, Morton Goldberg Professorship, the NIH Director's Pioneer Award, and the Department of Defense.

REFERENCES AND NOTES

1. Anderson JM, Inflammatory response to implants. ASAIO Trans. 34, 101–107 (1988). [PubMed: 3285869]
2. Singh J, Inaty H, Mukhopadhyay S, Mehta AC, Chronic pulmonary silicone embolism from breast augmentation is not a common finding in explanted lungs. Pulm. Med. 2018, 2987072 (2018).
3. Coroneos CJ, Selber JC, Offodile AC, Butler CE, Clemens MW, US FDA breast implant postapproval studies: Long-term outcomes in 99,993 patients. Ann. Surg. 269, 30–36 (2019). [PubMed: 30222598]
4. Hart AM, Lechowicz MJ, Peters KK, Holden J, Carlson GW, Breast implant–associated anaplastic large cell lymphoma: Report of 2 cases and review of the literature. Aesthet. Surg. J. 34, 884–894 (2014). [PubMed: 24938778]
5. Chen VW, Hoang D, Clancy S, Breast implant-associated bilateral B-cell lymphoma. Aesthet. Surg. J 40, NP52–NP58 (2018).
6. Shahriari N, Ferenczi K, Heald PW, Breast implant-associated anaplastic large cell lymphoma: A review and assessment of cutaneous manifestations. Int. J. Womens Dermatol. 3, 140–144 (2017). [PubMed: 28831423]
7. Marchant R, Hiltner A, Hamlin C, Rabinovitch A, Slobodkin R, Anderson JM, In vivo biocompatibility studies. I. The cage implant system and a biodegradable hydrogel. J. Biomed. Mater. Res 17, 301–325 (1983). [PubMed: 6841371]
8. Anderson JM, Rodriguez A, Chang DT, Foreign body reaction to biomaterials. Semin. Immunol. 20, 86–100 (2008). [PubMed: 18162407]
9. Ratner BD, Surface characterization of biomaterials by electron spectroscopy for chemical analysis. Ann. Biomed. Eng 11, 313–336 (1983). [PubMed: 6670788]

10. Anderson JM, McNally AK, Biocompatibility of implants: Lymphocyte/macrophage interactions. Semin. Immunopathol. 33, 221–233 (2011). [PubMed: 21271251]
11. Baht GS, Vi L, Alman BA, The role of the immune cells in fracture healing. Curr. Osteoporos. Rep 16, 138–145 (2018). [PubMed: 29508143]
12. Liao W, Hei TK, Cheng SK, Radiation-induced dermatitis is mediated by IL17- expressing γδ T Cells. Radiat. Res. 187, 454–464 (2017). [PubMed: 28406748]
13. Sadtler K, Estrellas K, Allen BW, Wolf MT, Fan H, Tam AJ, Patel CH, Luber BS, Wang H, Wagner KR, Powell JD, Housseau F, Pardoll DM, Elisseeff JH, Developing a pro-regenerative biomaterial scaffold microenvironment requires T helper 2 cells. Science 352, 366–370 (2016). [PubMed: 27081073]
14. Wolfram D, Rabensteiner E, Grundtman C, Böck G, Mayerl C, Parson W, Almanzar G, Hasenöhrl C, Piza-Katzer H, Wick G, T regulatory cells and TH17 cells in peri-silicone implant capsular fibrosis. Plast. Reconstr. Surg. 129, 327e–337e (2012).
15. Hotchkiss KM, Clark NM, Olivares-Navarrete R, Macrophage response to hydrophilic biomaterials regulates MSC recruitment and T-helper cell populations. Biomaterials 182, 202–215 (2018). [PubMed: 30138783]
16. Garay RP, El-Gewely R, Armstrong JK, Garratty G, Richette P, Antibodies against polyethylene glycol in healthy subjects and in patients treated with PEG-conjugated agents. Expert Opin. Drug Deliv. 9, 1319–1323 (2012). [PubMed: 22931049]
17. Wilson MS, Madala SK, Ramalingam TR, Gochuico BR, Rosas IO, Cheever AW, Wynn TA, Bleomycin and IL-1β–mediated pulmonary fibrosis is IL-17A dependent. J. Exp. Med. 207, 535–552 (2010). [PubMed: 20176803]
18. Childs BG, Durik M, Baker DJ, van Deursen JM, Cellular senescence in aging and age-related disease: From mechanisms to therapy. Nat. Med. 21, 1424–1435 (2015). [PubMed: 26646499]
19. Ritschka B, Storer M, Mas A, Heinzmann F, Ortells MC, Morton JP, Sansom OJ, Zender L, Keyes WM, The senescence-associated secretory phenotype induces cellular plasticity and tissue regeneration. Genes Dev. 31, 172–183 (2017). [PubMed: 28143833]
20. Watanabe S, Kawamoto S, Ohtani N, Hara E, Impact of senescence-associated secretory phenotype and its potential as a therapeutic target for senescence-associated diseases. Cancer Sci. 108, 563–569 (2017). [PubMed: 28165648]
21. Schafer MJ, White TA, Iijima K, Haak AJ, Ligresti G, Atkinson EJ, Oberg AL, Birch J, Salmonowicz H, Zhu Y, Mazula DL, Brooks RW, Fuhrmann-Stroissnigg H, Pirtskhalava T, Prakash YS, Tchkonia T, Robbins PD, Aubry MC, Passos JF, Kirkland JL, Tschumperlin DJ, Kita H, LeBrasseur NK, Cellular senescence mediates fibrotic pulmonary disease. Nat. Commun. 8, 14532 (2017). [PubMed: 28230051]
22. Chalan P, van den Berg A, Kroesen B-J, Brouwer L, Boots A, Rheumatoid arthritis, immunosenescence and the hallmarks of aging. Curr. Aging Sci. 8, 131–146 (2015). [PubMed: 26212057]
23. Palmer AK, Tchkonia T, LeBrasseur NK, Chini EN, Xu M, Kirkland JL, Cellular senescence in Type 2 diabetes: A therapeutic opportunity. Diabetes 64, 2289–2298 (2015). [PubMed: 26106186]
24. Katsuumi G, Shimizu I, Yoshida Y, Minamino T, Vascular senescence in cardiovascular and metabolic diseases. Front. Cardiovasc. Med. 5, 18 (2018). [PubMed: 29556500]
25. Lagares D, Santos A, Grasberger PE, Liu F, Probst CK, Rahimi RA, Sakai N, Kuehl T, Ryan J, Bhola P, Montero J, Kapoor M, Baron M, Varelas X, Tschumperlin DJ, Letai A, Tager AM, Targeted apoptosis of myofibroblasts with the BH3 mimetic ABT-263 reverses established fibrosis. Sci. Trans. Med 9, eaal3765 (2017).
26. Li Q, Ding S, Wang YM, Xu X, Shen Z, Fu R, Liu M, Hu C, Zhang C, Cao Q, Wang Y, Age-associated alteration in Th17 cell response is related to endothelial cell senescence and atherosclerotic cerebral infarction. Am. J. Transl. Res 9, 5160–5168 (2017). [PubMed: 29218113]
27. Harris TJ, Grosso JF, Yen H-R, Xin H, Kortylewski M, Albesiano E, Hipkiss EL, Getnet D, Goldberg MV, Maris CH, Housseau F, Yu H, Pardoll DM, Drake CG, Cutting edge: An in vivo requirement for STAT3 signaling in TH17 development and TH17-dependent autoimmunity. J. Immunol. 179, 4313–4317 (2007). [PubMed: 17878325]

28. Annunziato F, Romagnani C, Romagnani S, The 3 major types of innate and adaptive cell-mediated effector immunity. J. Allergy Clin. immunol 135, 626–635 (2015). [PubMed: 25528359]
29. Southern BD, Grove LM, Scheraga RG, Abraham S, Niese KA, Mansoor S, Rosenfeld SS, Olman MA, in C78. FIBROSIS: MEDIATORS AND MODULATORS. (American Thoracic Society, 2017), p. A6422.
30. Meng X-M, Nikolic-Paterson DJ, Lan HY, TGF-β: The master regulator of fibrosis. Nat. Rev. Nephrol 12, 325–338 (2016). [PubMed: 27108839]
31. Chen CZC, Raghunath M, Focus on collagen: In vitro systems to study fibrogenesis and antifibrosis state of the art. Fibrogenesis Tissue Repair 2, 7 (2009). [PubMed: 20003476]
32. Veiseh O, Doloff JC, Ma M, Vegas AJ, Tam HH, Bader AR, Li J, Langan E, Wyckoff J, Loo S, Jhunjhunwala S, Chiu A, Siebert S, Tang K, Hollister-Lock J, Aresta-Dasilva S, Bochenek M, Mendoza-Elias J, Wang Y, Qi M, Lavin DM, Chen M, Dholakia N, Thakrar R, Lacík I, Weir GC, Oberholzer J, Greiner DL, Langer R, Anderson DG, Size- and shape-dependent foreign body immune response to materials implanted in rodents and non-human primates. Nat. Mater. 14, 643–651 (2015). [PubMed: 25985456]
33. Beckman EM, Porcelli SA, Morita CT, Behar SM, Furlong ST, Brenner MB, Recognition of a lipid antigen by CD1-restricted $\alpha\beta^+$ T cells. Nature 372, 691–694 (1994). [PubMed: 7527500]
34. Sutton CE, Lalor SJ, Sweeney CM, Brereton CF, Lavelle EC, Mills KHG, Interleukin-1 and IL-23 induce innate IL-17 production from γδ T cells, amplifying Th17 responses and autoimmunity. Immunity 31, 331–341 (2009). [PubMed: 19682929]
35. Pellicoro A, Ramachandran P, Iredale JP, Fallowfield JA, Liver fibrosis and repair: immune regulation of wound healing in a solid organ. Nat. Rev. Immunol 14, 181–194 (2014). [PubMed: 24566915]
36. Borthwick LA, Wynn TA, Fisher AJ, Cytokine mediated tissue fibrosis. Biochim. Biophys. Acta 1832, 1049–1060 (2013). [PubMed: 23046809]
37. Wu L, Ong SF, Talor MV, Barin JG, Baldeviano GC, Kass DA, Bedja D, Zhang H, Sheikh A, Margolick JB, Iwakura Y, Rose NR, Cihákova D, Cardiac fibroblasts mediate IL-17A–driven inflammatory dilated cardiomyopathy. J. Exp. Med 211, 1449–1464 (2014). [PubMed: 24935258]
38. Mi S, Li Z, Yang H-Z, Liu H, Wang J-P, Ma Y-G, Wang X-X, Liu H-Z, Sun W, Hu Z-W, Blocking IL-17A promotes the resolution of pulmonary inflammation and fibrosis via TGF-β1-dependent and-independent mechanisms. J. Immunol. 187, 3003–3014 (2011). [PubMed: 21841134]
39. Wolf MT, Carruthers CA, Dearth CL, Crapo PM, Huber A, Burnsed OA, Londono R, Johnson A, Daly KA, Stahl EC, Freund JM, Medberry CJ, Carey LE, Nieponice A, Amoroso NJ, Badylak SF, Polypropylene surgical mesh coated with extracellular matrix mitigates the host foreign body response. J. Biomed. Mater. Res. A 102, 234–246 (2014). [PubMed: 23873846]
40. Nelson G, Wordsworth J, Wang C, Jurk D, Lawless C, Martin-Ruiz C, von Zglinicki T, A senescent cell bystander effect: Senescence-induced senescence. Aging Cell 11, 345–349 (2012). [PubMed: 22321662]
41. Salama R, Sadaie M, Hoare M, Narita M, Cellular senescence and its effector programs. Genes Dev. 28, 99–114 (2014). [PubMed: 24449267]
42. Stein GH, Drullinger LF, Soulard A, Dulić V, Differential roles for cyclin-dependent kinase inhibitors p21 and p16 in the mechanisms of senescence and differentiation in human fibroblasts. Mol. Cell. Biol. 19, 2109–2117 (1999). [PubMed: 10022898]
43. Chang J, Wang Y, Shao L, Laberge R-M, Demaria M, Campisi J, Janakiraman K, Sharpless NE, Ding S, Feng W, Luo Y, Wang X, Aykin-Burns N, Krager K, Ponnappan U, Hauer-Jensen M, Meng A, Zhou D, Clearance of senescent cells by ABT263 rejuvenates aged hematopoietic stem cells in mice. Nat. Med. 22, 78–83 (2016). [PubMed: 26657143]
44. Silva MM, Modolin M, Faintuch J, Yamaguchi CM, Zandona CB, Cintra W Jr., Fujiwara H, Curi R, Gemperli R, Ferreira MC, Systemic inflammatory reaction after silicone breast implant. Aesthetic Plast. Surg. 35, 789–794 (2011). [PubMed: 21424173]
45. Wawrzynski J, Gil JA, Goodman AD, Waryasz GR, Hypersensitivity to orthopedic implants: A review of the literature. Rheumatol. Ther. 4, 45–56 (2017). [PubMed: 28364382]

46. Brodbeck WG, Voskerician G, Ziats NP, Nakayama Y, Matsuda T, Anderson JM, In vivo leukocyte cytokine mRNA responses to biomaterials are dependent on surface chemistry. J. Biomed. Mater. Res. A 64, 320–329 (2003). [PubMed: 12522819]
47. Chen J, Crispín JC, Tedder TF, Lucca JD, Tsokos GC, B cells contribute to ischemia/reperfusion-mediated tissue injury. J. Autoimmun. 32, 195–200 (2009). [PubMed: 19342197]
48. Julier Z, Park AJ, Briquez PS, Martino MM, Promoting tissue regeneration by modulating the immune system. Acta Biomater. 53, 13–28 (2017). [PubMed: 28119112]
49. Doloff JC, Veiseh O, Vegas AJ, Tam HH, Farah S, Ma M, Li J, Bader A, Chiu A, Sadraei A, Aresta-Dasilva S, Griffin M, Jhunjhunwala S, Webber M, Siebert S, Tang K, Chen M, Langan E, Dholokia N, Thakrar R, Qi M, Oberholzer J, Greiner DL, Langer R, Anderson DG, Colony Stimulating Factor-1 Receptor is a central component of the foreign body response to biomaterial implants in rodents and non-human primates. Nat. Mater. 16, 671–680 (2017). [PubMed: 28319612]
50. Meraz IM, Melendez B, Gu J, Wong STC, Liu X, Andersson HA, Serda RE, Activation of the inflammasome and enhanced migration of microparticle-stimulated dendritic cells to the draining lymph node. Mol. Pharm. 9, 2049–2062 (2012). [PubMed: 22680980]
51. Zhang Y, Liao K, Li C, Lai ACK, Foo J-J, Chan V, Progress in integrative biomaterialsystems to approach three-dimensional cell mechanotransduction. Bioengineering 4, 72 (2017).
52. Regier MC, Montanez-Sauri SI, Schwartz MP, Murphy WL, Beebe DJ, Sung KE, The influence of biomaterials on cytokine production in 3D cultures. Biomacromolecules 18, 709–718 (2017). [PubMed: 28157290]
53. Kreeger PK, Strong LE, Masters KS, Engineering approaches to study cellular decision making. Annu. Rev. Biomed. Eng 20, 49–72 (2018). [PubMed: 29328778]
54. Duscher D, Maan ZN, Wong VW, Rennert RC, Januszyk M, Rodrigues M, Hu M, Whitmore AJ, Whittam AJ, Longaker MT, Gurtner GC, Mechanotransduction and fibrosis. J. Biomech. 47, 1997–2005 (2014). [PubMed: 24709567]
55. Cipolla E, Fisher AJ, Gu H, Mickler EA, Agarwal M, Wilke CA, Kim KK, Moore BB, Vittal R, IL-17A deficiency mitigates bleomycin-induced complement activation during lung fibrosis. FASEB J. 31, 5543–5556 (2017). [PubMed: 28821630]
56. Meng F, Wang K, Aoyama T, Grivennikov SI, Paik Y, Scholten D, Cong M, Iwaisako K, Liu x., Zhang M, Österreicher CH, Stickel F, Ley K, Brenner DA, Kisseleva T, Interleukin-17 signaling in inflammatory cells, Kupffer cells and hepatic stellate cells exacerbates liver fibrosis. Gastroenterology 143, 765–776.e3 (2012). [PubMed: 22687286]
57. Sadtler K, Wolf MT, Ganguly S, Moad CA, Chung L, Majumdar S, Housseau F, Pardoll DM, Elisseeff JH, Divergent immune responses to synthetic and biological scaffolds. Biomaterials 192, 405–415 (2019). [PubMed: 30500722]
58. Xu M, Pirtskhalava T, Farr JN, Weigand BM, Palmer AK, Weivoda MM, Inman CL, Ogrodnik MB, Hachfeld CM, Fraser DG, Onken JL, Johnson KO, Verzosa GC, Langhi LGP, Weigl M, Giorgadze N, LeBrasseur NK, Miller JD, Jurk D, Singh RJ, Allison DB, Ejima K, Hubbard GB, Ikeno Y, Cubro H, Garovic VD, Hou X, Weroha SJ, Robbins PD, Niedernhofer LJ, Khosla S, Tchkonia T, Kirkland JL, Senolytics improve physical function and increase lifespan in old age. Nat. Med. 24, 1246–1256 (2018). [PubMed: 29988130]
59. López-Otín C, Blasco MA, Partridge L, Serrano M, Kroemer G, The hallmarks of aging. Cell 153, 1194–1217 (2013). [PubMed: 23746838]
60. Kirkland JL, Tchkonia T, Cellular senescence: A translational perspective. EBioMedicine 21, 21–28 (2017). [PubMed: 28416161]
61. Justice JN, Nambiar AM, Tchkonia T, Le Brasseur NK, Pascual R, Hashmi SK, Prata L, Masternak MM, Kritchevsky SB, Musi N, Kirkland JL, Senolytics in idiopathic pulmonary fibrosis: Results from a first-in-human, open-label, pilot study. EBioMedicine 40, 554–563 (2019). [PubMed: 30616998]
62. Jeon OH, Kim C, Laberge R-M, Demaria M, Rathod S, Vasserot AP, Chung JW, Kim DH, Poon Y, David N, Baker DJ, van Deursen JM, Campisi J, Elisseeff JH, Local clearance of senescent cells attenuates the development of post-traumatic osteoarthritis and creates a pro-regenerative environment. Nat. Med. 23, 775–781 (2017). [PubMed: 28436958]

63. Siskind GW, Paul WE, Benacerraf B, Studies on the effect of the carrier molecule on antihapten antibody synthesis. I. Effect of carrier on the nature of the antibody synthesized. J. Exp. Med. 123, 673–688 (1966). [PubMed: 4160398]

64. Dintzis HM, Dintzis RZ, Vogelstein B, Molecular determinants of immunogenicity: The immunon model of immune response. Proc. Natl. Acad. Sci. U.S.A. 73, 3671–3675 (1976). [PubMed: 62364]

65. Mitchelson AJ, Wilson CJ, Mihalko WM, Grupp TM, Manning BT, Dennis DA, Goodman SB, Tzeng TH, Vasdev S, Saleh KJ, Biomaterial hypersensitivity: Is it real? Supportive evidence and approach considerations for metal allergic patients following total knee arthroplasty. Biomed Res. Int. 2015, 137287 (2015).

66. Zhang P, Sun F, Liu S, Jiang S, Anti-PEG antibodies in the clinic: Current issuesand beyond PEGylation. J. Control. Release 244, 184–193 (2016). [PubMed: 27369864]

67. Lepore M, Mori L, De Libero G, The conventional nature of non-MHC-restricted T cells. Front. Immunol. 9, 1365 (2018). [PubMed: 29963057]

68. Sicari BM, Agrawal V, Siu BF, Medberry CJ, Dearth CL, Turner NJ, Badylak SF, A murine model of volumetric muscle loss and a regenerative medicine approach for tissue replacement. Tissue Eng. Part A 18, 1941–1948 (2012). [PubMed: 22906411]

69. Livak KJ, Schmittgen TD, Analysis of relative gene expression data using real-time quantitative PCR and the 2−ΔΔCT method. Methods 25, 402–408 (2001). [PubMed: 11846609]

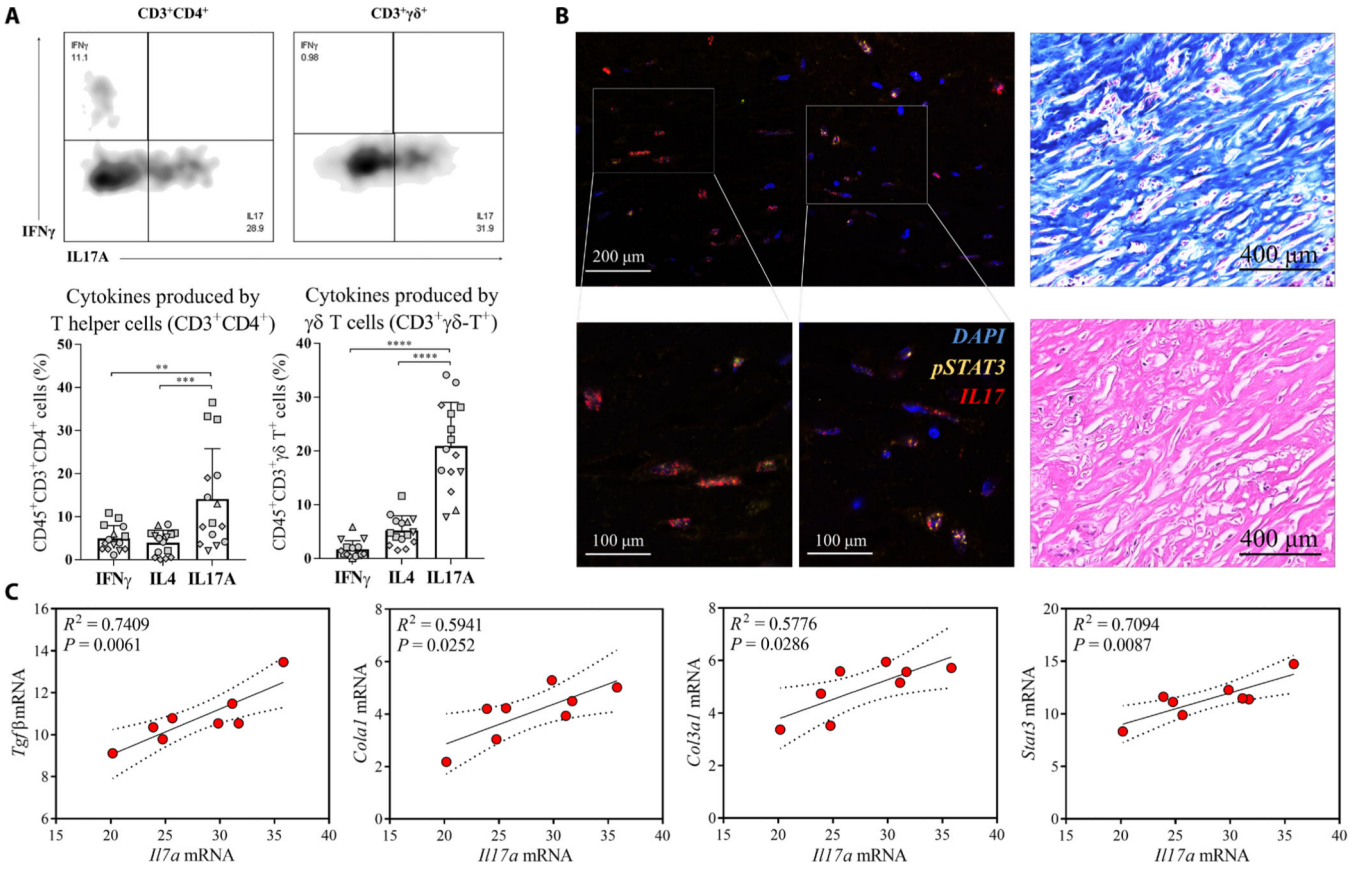

Fig. 1. IL17 is secreted by γδ$^+$ T cells and CD4$^+$ T cells in tissue around human breast implants and correlates with expression of fibrosis markers.

Tissue samples surrounding 12 surgically removed breast implants were evaluated by flow cytometry and gene expression analysis. (**A**) Flow cytometry analysis measuring different cytokines produced by T helper cells (CD45+Thy1.2$^+$CD3$^+$CD4$^+$) and γδ$^+$ T cells (CD45$^+$Thy1.2$^+$CD3$^+$γδ$^+$) from breast implant–associated tissue. Samples from individual patients are designated with different shapes. (**B**) (Left) Immunofluorescence staining for pSTAT3 (green) and IL17 (red) in the fibrous capsule surrounding excised breast implants. (Right) Staining of the fibrous capsule with hematoxylin and eosin and with Masson's trichrome stain for collagen. (**C**) qRT-PCR analysis shows *Il17a* mRNA expression and its correlation with mRNA expression for the fibrosis-associated proteins collagen type I (*Col1a1*), collagen type III (*Col3a1*), and *Tgfβ*. In addition, correlations between *Il17a* and *Stat3* mRNA expression were evaluated. Data are mean ± SD, $n = 5$ (A), $n = 8$ (C). ****$P <$ 0.0001, ***$P < 0.001$, **$P < 0.01$, and *$P < 0.05$ by analysis of variance (ANOVA) (A) or linear regression (C).

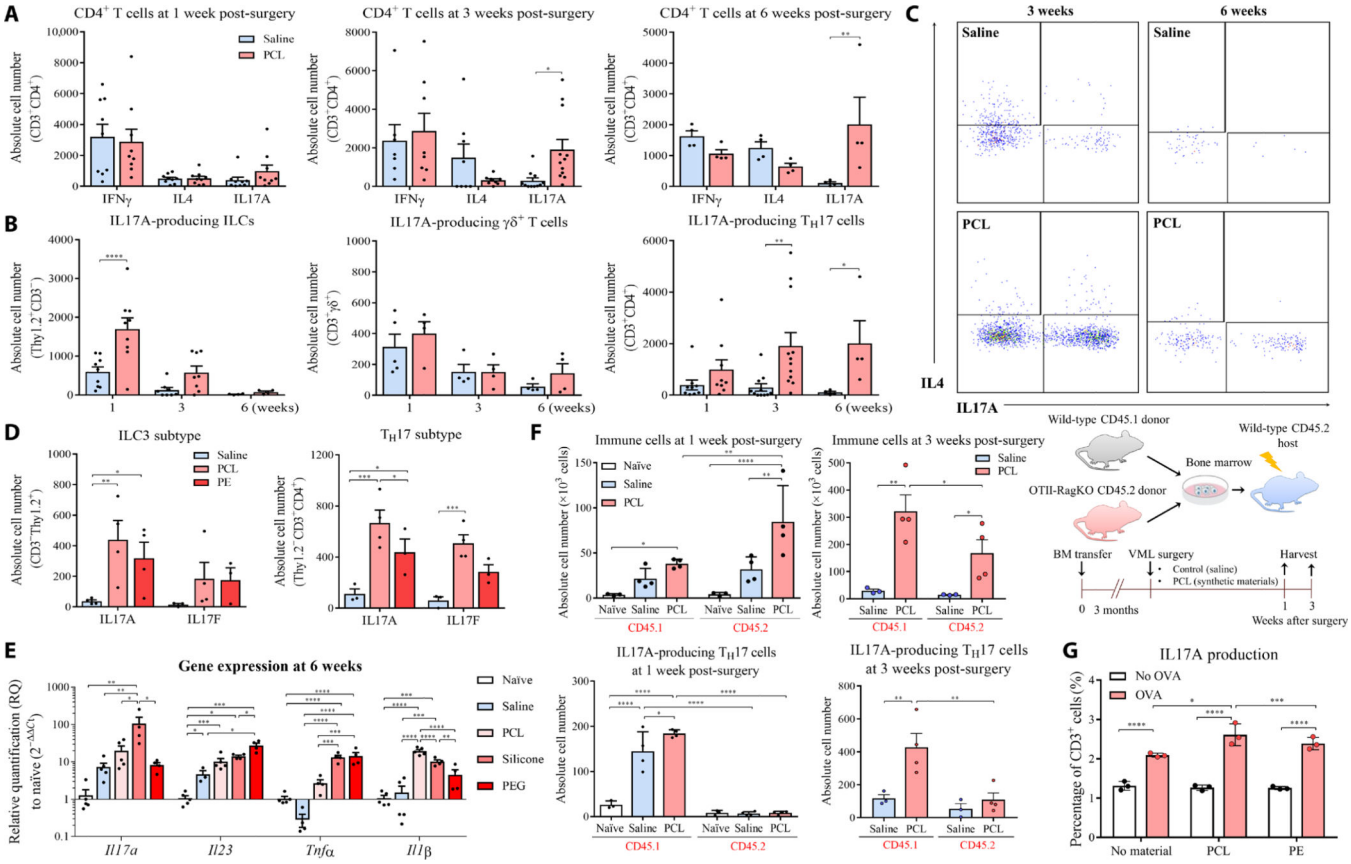

Fig. 2. Implanted synthetic materials induce an IL17 immune response in mice.

(**A**) C57BL/6 mice received an injury to their quadriceps muscle and were subsequently implanted with PCL or PE synthetic material particles or saline as a control. Numbers of T cells secreting IFN**γ**, IL4, and IL17A were quantified at different time points by flow cytometry at 1, 3, or 6 weeks after surgery. (**B**) Kinetics of IL17A expression by different cell types, including innate lymphoid cells (ILCs), $\gamma\delta^+$ T cells, and $CD4^+$ T helper cells over time since surgery. (**C**) Representative flow cytometry plots of IL17A production by CD4+ T cells at 3 and 6 weeks after surgery. (**D**) IL17A and IL17F cytokines were quantified in ILCs and T_H17 cells by flow cytometry in muscles implanted with PCL or PE particles at 3 weeks after surgery. (**E**) qRT-PCR analysis of mRNA expression for *Il17a* and other inflammatory genes such as *Il1*β, *Il23*, and *Tnf*α in tissue surrounding implanted PCL, PEG, or silicone particles 6 weeks after implantation. (**F**) Experi- mental overview of the bone marrow (BM) chimera studies. The total number of immune cells and T_H17 cells from CD45.1 (wild-type donor) and CD45.2 (OTII-$Rag^{-/-}$ donor) bone marrow chimera mice 1 and 3 weeks after volumetric muscle loss and synthetic material implantation was measured. The percentage of CD45.1 and CD45.2 immune cells that were T_H17 cells was calculated. (**G**) Splenocytes from OTII transgenic mice were cultured with different materials (PCL or PE) and OVA antigen. Production of IL17A was quantified by intracellular staining. Data are displayed as relative quantification (RQ) to healthy unimplanted mouse tissue for (E). Data are mean ± SD, $n = 4$ to 12 (A and B), $n = 4$ (D and E), $n = 3$ (G). ****$P < 0.0001$, ***$P < 0.001$, **$P < 0.01$, and *$P < 0.05$ by ANOVA for data in (A), (B), and (D) to (G).

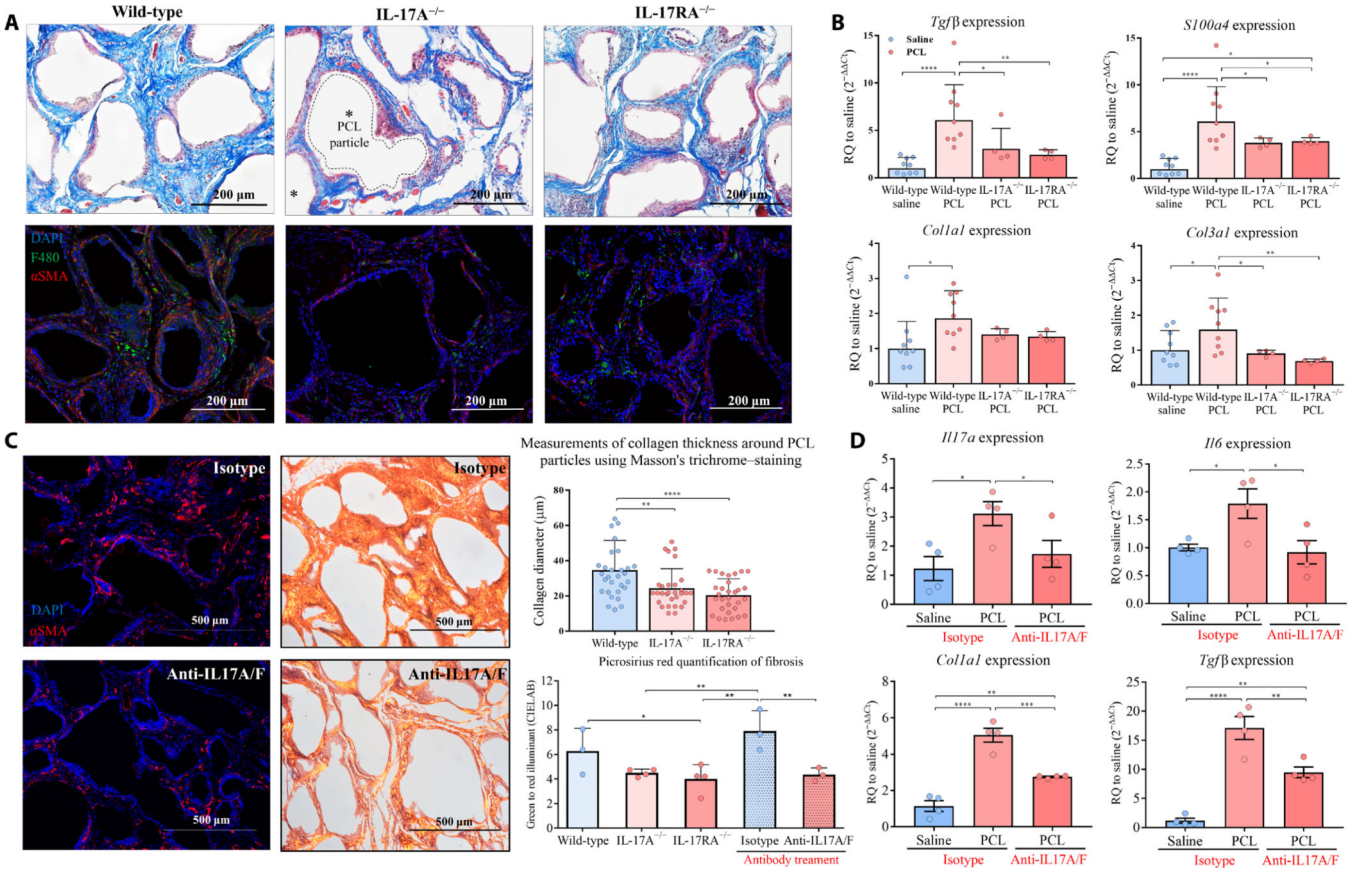

Fig. 3. IL17 inhibition reduces the fibrotic response to synthetic materials.

PCL was implanted in knockout mice that lacked either IL17A or the IL17RA receptor.(A) Histochemical staining of implants for collagen (Masson's trichrome stain, top row) and immunofluorescence staining for the macrophage marker F4/80 and fibrosis- associated protein αSMA (bottom row) were performed at 12 weeks after surgery. (**B**) qRT-PCR mRNA expression of fibrotic markers including TGFβ, S100a4, and collagen III was analyzed in wild-type, IL17A$^{-/-}$, and IL17RA−/− mice at 6 weeks after surgery. (**C**) Co-administration of IL17A and IL17F neutralizing antibodies (100 0μg/ml each) or isotype antibody control (mouse IgG1) was introduced intraperitoneally for mice with PCL implanted 4 weeks previously. To evaluate the degree of fibrosis, tissues were harvested 6 weeks after surgery for histological assessment. (Left) Immunofluorescence staining showed reduced expression of αSMA in mice given the antibody treatment compared to those receiving the isotype antibody control. (Right) Picrosirius red stain showed the spectrum of color (green to red) relative to the degree of collagen density (thinnest to thickest, respectively); green to red illuminant was quantified by CIELAB (right images). Thickness of the fibrous capsule in wild-type and IL17-deficient mice was also measured in Masson Trichrome images. (**D**) qRT-PCR mRNA expression of *Il17a*, *Il6*, *Tgf*β, and *Col1a1* in tissues of mice treated with neutralizing antibodies against IL17A and IL17F compared to tissues from mice treated with isotype antibody control at 6 weeks after surgery. Data are displayed as relative quantification to a saline control in (B) and (D). Data are mean ± SD, *n*

= 9 (wild-type mice), $n = 4$ (IL17-deficient mice). ****$P < 0.0001$, ***$P < 0.001$, **$P < 0.01$, and *$P < 0.05$ by ANOVA for data in (B) to (D).

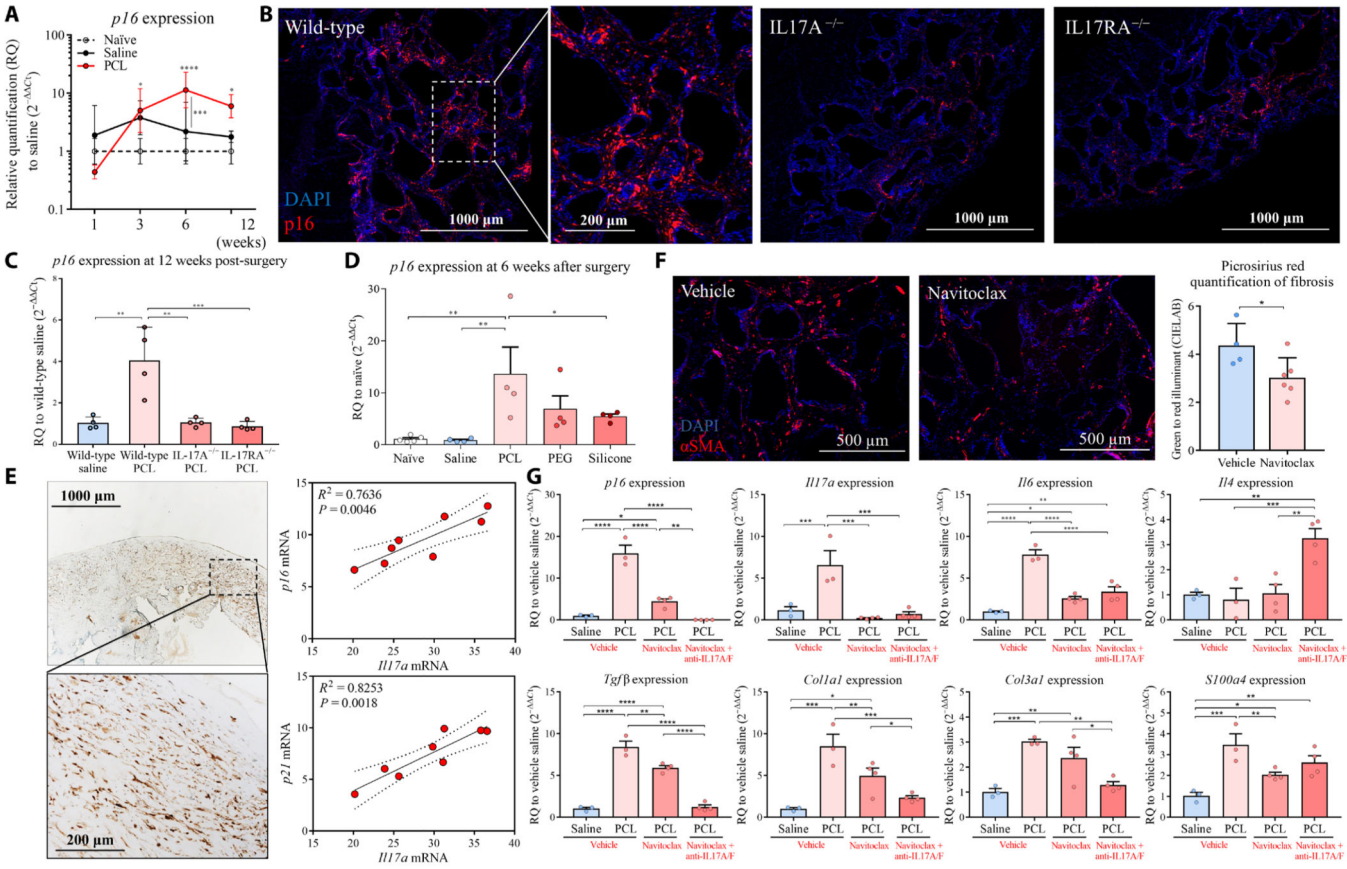

Fig. 4. p16^{INK4a} senescent cell development is abrogated in IL17A$^{-/-}$ and IL17RA$^{-/-}$ mice implanted with synthetic materials.

(**A**) qRT-PCR mRNA expression of *p16^{INK4a}* over time since surgical implantation of a synthetic material or saline normalized to a naïve tissue control (no surgery). (**B**) Immunofluorescence staining of p16^{INK4a} (red) in tissue surrounding implants from wild-type mice, IL17A$^{-/-}$ mice, and IL17RA$^{-/-}$ mice. (**C**) qRT-PCR analyses of p16^{INK4a} mRNA expression in tissue surrounding PCL implants from wild-type mice, IL17A$^{-/-}$mice, and IL17RA$^{-/-}$ mice at 12 weeks after injury. (**D**) qRT-PCR mRNA expression for p16^{INK4a} comparing tissue surrounding different synthetic materials (PCL, PE, and silicone) at 6 weeks after surgery. (**E**) Immunohistochemistry images of p16^{INK4a} expression in cells in the fibrotic capsule surrounding human breast implants. Linear regression shows the correlation between *Il17a* mRNA expression and *p16^{INK4a}* and *p21* mRNA expression. Dotted lines indicated the 95% confidence intervals (CI) of the fitted line. (**F**) Navitoclax (ABT-263) was administrated to mice 4 weeks after surgery to eliminate senescent cells. Muscles were harvested at 6 weeks after surgery for histological staining. Immunofluorescent images of αSMA expression in tissue surrounding implants from mice treated with navitoclax or DMSO vehicle control are shown. Quantification of Picrosirius red staining to measure collagen density is shown. (**G**) Implanted mice received navitoclax treatment alone or in combination with neutralizing antibodies against IL17A and IL17F at 4 weeks after surgery. Tissue was harvested at 6 weeks after surgery to evaluate mRNA expression of *p16INK4a*, *Il17a*, *Il6*, *Il4*, *Tgf*β, *S100a4*, *Col1a1*, and *Col3a1*. Data are mean ±

SD, $n = 3$ to 5 (A, C to E, and G), $n = 8$ (F). ****$P < 0.0001$, ***$P < 0.001$, **$P < 0.01$, and *$P < 0.05$ by ANOVA for data in (A), (C) to (E), and (G) and by linear regression for data in (F).